Nanostructures

DOI: 10.1002/anie.200905678

Photoresponsive Supramolecular Organometallic Nanosheets Induced by $Pt^{II}\cdots Pt^{II}$ and C–H···π Interactions**

Yong Chen, Kai Li, Wei Lu, Stephen Sin-Yin Chui, Chun-Wah Ma, and Chi-Ming Che**

While graphene, a carbon-based two-dimensional nanomaterials, has received an upsurge of interest,[1] self-assembly of small organic and organometallic molecules into 2D nanostructures could also be harnessed to develop new classes of functional supramolecular nanomaterials.[2] In principle, quasi-2D lamellae or nanosheets are planar structures having a thickness less than 100 nm and lateral dimensions a few orders of magnitude greater than their thickness. Control over the bilateral intermolecular noncovalent interactions is anticipated to organize small molecules into regular 2D nanostructures, which has been a formidable challenge yet to be achieved. Recently, Shelnutt and co-workers obtained discrete porphyrin nanosheets reprecipitated from their solutions;[3] Sathish and co-workers constructed hexagonal C_{60} nanosheets using a liquid–liquid interfacial precipitation method;[4] the groups of Yao[5] and Hu[6] prepared single-crystalline nanosheets of polycyclic aromatics using a surfactant-assisted reprecipitation and a physical vapor transporting method, respectively; and Zhang and co-workers suggested that molecules with intramolecular charge-transfer dipole moments could be grown into quasi-2D nanostructures.[7] Moreover, some amphiphiles and organogelators were found to self-organize into sheet-like nanostructures in contact with solvents.[8] Despite these advances, template- and surfactant-free synthesis of free-standing, crystalline, and optoelectronically active nanosheets from small molecules remains elusive.

Square-planar platinum(II) complexes containing π-conjugated ligands are particularly attractive building blocks for self-assembly reactions, because cofacial molecular aggregation can maximize the orbital interactions between two π systems, thus leading to rich photophysical and photochemical properties that can be harnessed for optoelectronic applications and light-energy conversion reactions.[9] Intermolecular $Pt^{II}\cdots Pt^{II}$ interactions play a key role in the close packing of molecules. To date, quasi-one-dimensional nanowires have been obtained by self-organization of organoplatinum(II) complexes, presumably owing to the fact that molecular propagation is faster along the $Pt^{II}\cdots Pt^{II}$ chain axis than in the lateral directions. We and others have taken advantage of this anisotropic growth mechanism to assemble cationic organoplatinum(II) salts into nanostructures with luminescent, semiconducting, liquid crystalline, and gelating properties.[10] Herein we report free-standing and crystalline nanosheets self-assembled from neutral pincer-type[11] cyclometalated platinum(II) aryl acetylides. Indeed, intermolecular $Pt^{II}\cdots Pt^{II}$ and C–H···π(C≡C)[12] interactions in an orthogonal configuration account for the quasi-2D molecular organization herein. Notably, these organometallic nanosheets luminesce in the red to near infrared (NIR) region, and their electronic conductivity can be modulated by visible-light irradiation.

The charge-neutral organoplatinum(II) complexes herein, namely [4-R^1-(N^C^N)PtC≡CC_6H_4-4′-R^2] (**1**–**8**, N^CH^N = 1,5-bis(2′-pyridyl)benzene), were prepared in quantitative yields by stirring the corresponding precursor, [4-R^1-(N^C^N)PtCl] ($R^1 = CF_3$,[10g] H,[13a] or CH_3[13b]), and an excess of aryl acetylene in methanol in the presence of NaOH for one day at room temperature.[14] It is notable that when R^1 is CF_3, the solids of complexes **1**–**6** display various colors, depending on the substituent R^2 on the aryl acetylide ligand (Scheme 1). When R^2 is an electron-withdrawing group (CF_3 for **5** and NO_2 for **6**), an electron-donating group (OCH_3 for **3** and $N(CH_3)_2$ for **4**), or a relatively neutral group (H for **1** and F for **2**), the solid is bright yellow, deep red, or dark green in color, respectively. When R^1 is H or CH_3, no such color contrast was observed upon varying R^2 from electron-withdrawing to -donating groups; the solids are yellow in color, as depicted for complexes **7** and **8** in Scheme 1.

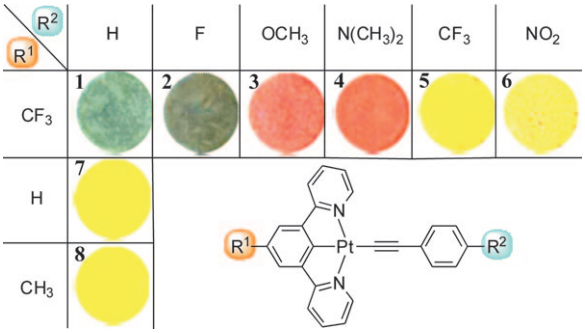

Scheme 1. Chemical structures and solid-state colors of **1**–**8**.

[*] Dr. Y. Chen, K. Li, Dr. W. Lu, Dr. S. S.-Y. Chui, C.-W. Ma, Prof. Dr. C.-M. Che
Department of Chemistry and
HKU-CAS Joint Laboratory on New Materials
The University of Hong Kong, Pokfulam Road, Hong Kong (China)
E-mail: luwei@hku.hk
cmche@hku.hk

[**] This work was supported by the "Nanotechnology Research Program" of the University Development Fund of The University of Hong Kong, and the Hong Kong Research Grants Council (HKU 7011/07P and 7008/09P). Y.C. thanks The University of Hong Kong for a Postdoctoral Fellowship. Thanks go to Dr. Zong-Xiang Xu, Frankie Yu-Fee Chan, and Amy Sui-Ling Wong for assistance in device fabrication and TEM/SEM observations. We thank Dr. Nianyong Zhu for solving the crystal structure of complex **7**.

Supporting information for this article is available on the WWW under http://dx.doi.org/10.1002/anie.200905678.

Colors of organoplatinum(II) complexes in the solid state are usually associated with intermetal interactions.[15] Various packing modes have been identified by X-ray crystallography for crystals of complexes **1** (Figure 1), **4** (Figure S1 in the Supporting Information), and **7** (Figure S2 in the Supporting Information), which appear as green, red, and yellow solids, respectively.[16] The salient features in the crystal structures of both **1** and **4** are the intermolecular $Pt^{II}\cdots Pt^{II}/\pi$–$\pi$ and C–H···π(C≡C) interactions in an orthogonal configuration.

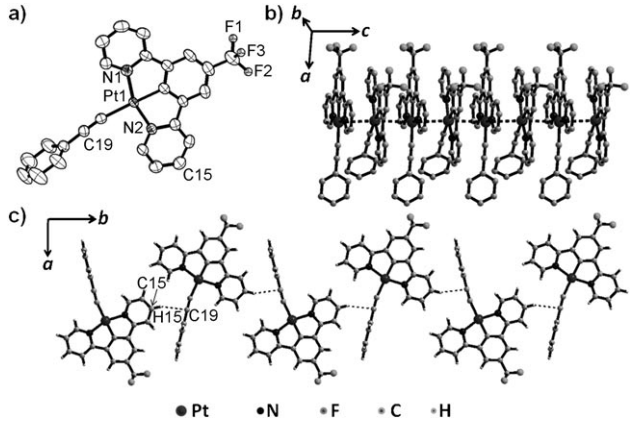

Figure 1. Crystal structure of **1**. a) Perspective view and b, c) packing diagrams. The three fluorine atoms of the CF_3 group are disordered. Dashed lines indicate intermolecular distances shorter than the sum of van der Waals radii.

Complex **1** crystallizes in an orthorhombic lattice without solvates. The acetylenic phenyl ring is perpendicular to the (N^C^N)Pt plane, and the latter is coplanar with the *ab* plane. Infinite $Pt^{II}\cdots Pt^{II}$ chains exist along the *c* axis, with a uniform intermetal contact of 3.383 Å (shorter than the sum of van der Waals radii of 3.44 Å) and a Pt-Pt-Pt angle of 172.85°. Neighboring molecules are arranged in a staggered fashion with a torsion angle of 49.4° around the Pt–Pt axis (Figure 1b). Intermolecular C–H···π interactions have been discerned between every two adjacent molecules along the *b* axis (Figure 1c), as indicated by a short contact of 2.691 Å between H15 of the (N^C^N) ligand and acetylenic C19 of another molecule, and a C15-H15-C19 angle of 159.6°. No short intermolecular contacts could be identified along the *a* axis.

Complex **4** crystallizes as thin plates with intrinsic twinning problems. Nevertheless, we were able to solve the crystal structure of **4** by direct methods based on a set of X-ray diffraction data with 87% completeness (see the Supporting Information for details). The crystal structure has a monoclinic space group with one half of a hexane solvate molecule per three crystallographically independent molecules of the complex. The (N^C^N)Pt planes of the these molecules are nearly coplanar with the [10–1] crystal faces (see the Supporting Information for diagrams). The intermetal distances between the two neighboring molecules are 3.229, 4.879, and 3.710 Å. Similar to crystal **1**, the intermolecular C–H···π(C≡C) interactions with a short contact distance of 2.646 Å and contact angle of 163.6° have been identified between every two adjacent molecules along the *c* axis.

In the crystal structure of **7**, the molecules pack into a dimeric structure in a head-to-tail fashion with an interplanar distance of approximately 3.4 Å and a shortest intermetal separation of 4.886 Å (see the Supporting Information), thus indicating a prominent π–π interaction but not a $Pt^{II}\cdots Pt^{II}$ interaction between the two paired molecules.

The reprecipitation method was adopted to prepare the nanostructures. Complexes **1**, **4**, and **7** are used as representative examples in the following description. The complex was dissolved in CH_2Cl_2 or THF to give a bright yellow solution (ca. 6.0 mM, 0.5 mL). Addition of 5 mL *n*-hexane or cyclohexane into the CH_2Cl_2 solution gave a green, red, or yellow suspension for **1** (Figure 2a), **4** (Figure 2g), and **7**, respectively. The nanostructures precipitated from the solvent upon long-term standing but can be re-dispersed upon shaking. No color or morphological changes were observed after months or even after boiling the suspensions.

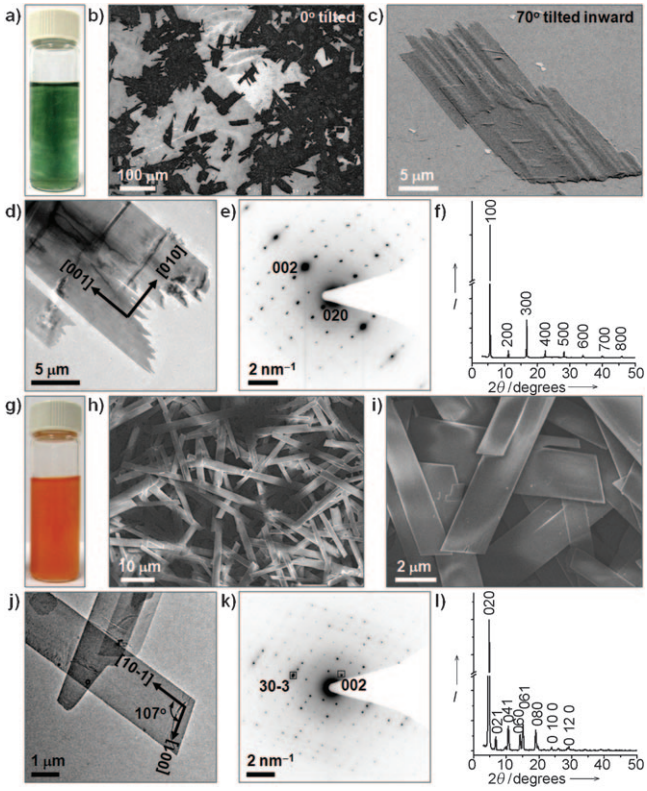

Figure 2. Characterization of nanosheets of **1** (a–f) and **4** (g–l). a, g) Photographs of dispersions in CH_2Cl_2/*n*-hexane (1:10 v/v). b, c, h, i) SEM images at different magnifications and tilt angles. d, e, j, k) TEM images and corresponding SAED patterns. The TEM images have been rotated 92° so that the diffraction pattern coincides in orientation with the image; f, l) Powder XRD patterns of thin films prepared by drop-casting of the dispersions.

Observations by scanning electron microscopy (SEM, Figure 2b, c) and transmission electron microscopy (TEM, Figure 2d) revealed that the as-prepared suspension of **1** contains 2D sheet-like nanostructures, irrespective of the

reprecipitation solvent system. Both the length and width of the sheets are tens of micrometers, while the average thickness is less than 50 nm, which has been further confirmed by atomic force microscopy (AFM, Figure S3 in the Supporting Information). Decreasing the complex concentration or changing the good solvent from CH_2Cl_2 to THF during reprecipitation can reduce the lateral dimensions while keeping the thickness of the nanosheets in the nanometer scale (Figure S4 in the Supporting Information). The selected area electron diffraction (SAED) pattern of a single nanosheet of **1** shows sharp and ordered spots (Figure 2e), which were successfully indexed according to the X-ray single-crystal structure of **1**. The *d* spacings of 9.59 and 3.40 Å correspond to the respective [020] and [002] Miller planes found in the crystal structure of **1**. By correlating the X-ray and electron diffraction data, the growth directions of the nanosheets coincide with the *c* and *b* axes, that is, the directions of extended $Pt^{II}\cdots Pt^{II}$ and C–H···π(C≡C) interactions, respectively. We suggest that these two types of intermolecular noncovalent interactions in an orthogonal configuration dictate the quasi-2D anisotropic growth of nanosheets. Complex **2** exhibits a similar capability to form nanosheets (Figure S5 in the Supporting Information) as complex **1**, except that the *d* spacing (9.38 Å) found for the [020] planes of nanosheets of **2** is smaller than that of **1** (9.59 Å).

Suspensions of **4** in CH_2Cl_2/*n*-hexane contained 2D plank-like nanosheets with a thickness, width, and length of less than 100 nm, 1–4 μm, and tens of micrometers, respectively. Sharp crystal facets with an angle of 107° were observed in both SEM and TEM images (Figure 2h–j). Sharp and ordered spots in the SAED pattern (Figure 2k) of a single nanosheet of **4** have been successfully indexed according to the X-ray single-crystal structure of **4**. The *d* spacings of 9.01 and 3.35 Å correspond to the respective [30−3] and [002] Miller planes found in the crystal structure of **4**. Similar to the study on nanosheets of **1**, complex **4** grew into a quasi-2D nanostructure coinciding with the [10−1] zone and *c* axis, that is, the direction for the extended $Pt^{II}\cdots Pt^{II}$/π–π stacking and C–H···π(C≡C) interactions, respectively. Using the same preparation protocol, complexes **3**, **5**, and **6** form quasi-1D nanowires or nanofibers, whereas complexes **7** and **8** form mixtures of nanoparticles and nanobelts (see the Supporting Information for micrographs).

The nanosheets of complexes **1** and **4** can be transferred onto a flat substrate to form layered structures. The drop-cast films of **1** on a glass slide exhibit metallic luster, and the powder X-ray diffraction (XRD) pattern of this film (Figure 2f) shows only [*h*00] peaks at $2\theta = 5.59$, 11.19, 16.81, 22.48, 28.20, 33.98, 39.88, and 45.86° ($d = 15.80$, 7.90, 5.27, 3.95, 3.16, 2.64, 2.26, and 1.98 Å, respectively), thus indicating a highly ordered alignment of molecules and the formation of a layered structure. It is evident that the nanosheets of **1** are preferentially oriented with *bc* planes of the crystal lattice parallel to the substrate surface. The powder XRD pattern of a drop-cast film of **4** shows only [0*k*0] and [0*k*1] (*k* is an even number) peaks (Figure 2l), thus indicating a preferred orientation of the nanosheets of **4** with *ac* planes of the crystal lattice parallel to the substrate surface.

The above-mentioned film of **1** displayed a low-energy absorption band at λ_{max} 720 nm and a near infrared (NIR) emission at λ_{max} 822 nm (Figure 3a). Both the low-energy absorption and emission are associated with the extended

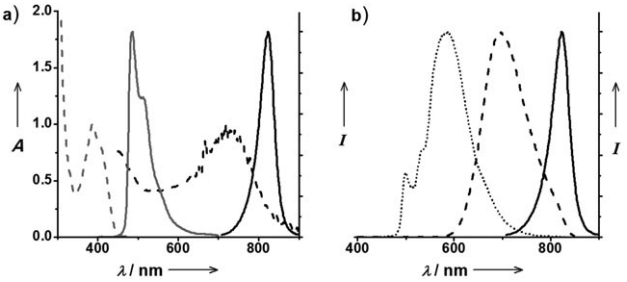

Figure 3. a) Absorption (dashed lines) and emission (solid lines) spectra of complex **1** in film (black lines) and in CH_2Cl_2 solution (gray lines). b) Normalized room-temperature solid-state emission spectra of complexes **1** (solid line), **4** (dashed line), and **7** (dotted line).

$Pt^{II}\cdots Pt^{II}$ chains found in the crystal structure of **1**.[8,9] In contrast, a diluted solution of **1** in CH_2Cl_2 is almost colorless, with the lowest absorption band at 387 nm; it luminesces with an emission maximum at 486 nm (Figure 3a). Again complexes **1**, **4**, and **7** are used to compare the spectroscopic properties in solution and in the solid state. Upon excitation at 365 nm, **1**, **4**, and **7** in diluted CH_2Cl_2 solutions (concentration ca. 2.0×10^{-5} mol dm^{-3}) at 298 K show intense emissions with λ_{max} (lifetime, quantum yield) at 486 (1.7 μs, 29%), 480 (3.8 μs, 8%), and 496 nm (2.6 μs, 52%), respectively. These photophysical properties are typical for pincer-type cyclometalated platinum(II) complexes.[13b,c] Powder samples of **1** and **4** at room temperature show structureless emissions at λ_{max} 819 and 702 nm (Figure 3b), respectively, which can be assigned to triplet metal-metal-to-ligand charge-transfer (^{3}MMLCT) excited states[9,10] associated with $Pt^{II}\cdots Pt^{II}$ interactions found in the crystal structures of **1** and **4**. A powder sample of **7** at room temperature exhibits a broad emission with λ_{max} at 587 nm superimposed by vibronically structured bands on the high-energy side (Figure 3b). We ascribe the high-energy emission in the region of 480–550 nm to triplet metal-to-ligand charge-transfer (^{3}MLCT) excited states [(5d)Pt→π*(cyclometalated ligand)] and the low-energy band at λ_{max} 587 nm to a triplet ππ*excimer.

We tested the charge-transporting properties of nanosheets of **1** using a bottom-contact field-effect transistor (FET) configuration. A suspension was drop-cast onto a prepatterned silicon wafer, thus making a couple of nanosheets to bridge interdigitated electrodes with a channel length of approximately 6 μm (Figure 4a). The output characteristics (Figure 4b) of this device revealed that these nanosheets behave as a p-type, hole-transporting semiconductor. A transient channel current was recorded with this device at $V_{DS} = V_G = \pm 40$ V and with a 40 mW cm^{-2} white light switching on and off every five seconds in a 90 s period. As shown in Figure 4c, the conductivity of these nanosheets showed reversible responses towards light irradiation. Both forward and backward currents were enhanced when the light was on, indicating that carrier density of both electron and

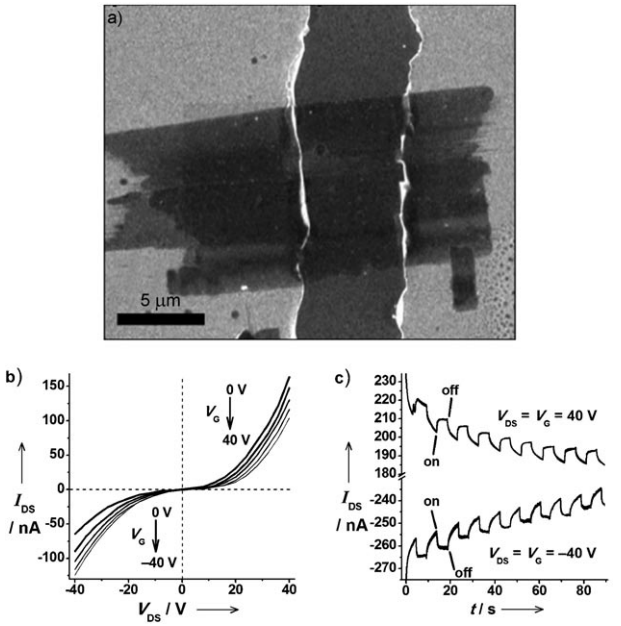

Figure 4. a) SEM image of a bottom-contact FET device with nanosheets of **1** as semiconducting materials. b) Output characteristics (I_{DS} vs. V_{DS}). c) Transient measurement ($V_{DS} = V_G = \pm 40$ V) of the FET device. The transient channel current was recorded with a 40 mW cm^{-2} light switching on and off every five seconds in a 90 second period. I_{DS} = drain–source current, V_{DS} = drain–source voltage, V_G = gate voltage.

hole are increased by photoexcitation of the organoplatinum(II)-based nanomaterials. We tested a total of five devices and found that the modulation of conductivity with light was reproducible. Although the performance of these photoresponsive transistors[17] has not been optimized, the photoresponsive properties of the nanosheets are promising for organometallic-based optoelectronics. No charge accumulation in the initial several seconds was observed. This finding is consistent with the charge-neutral nature of complex **1** and is in contrast to the previously reported FET device with cationic platinum(II) salts as semiconductors.[10a,e,g]

In conclusion, charge-neutral organoplatinum(II) complexes can self-assemble into quasi-2D nanostructures that display near infrared phosphorescence and light-modulated conductivity. The molecular organization in the nanosheets is attributed to orthogonal $Pt^{II}\cdots Pt^{II}$ and C–H$\cdots\pi$(C≡C) interactions. This work highlights that phosphorescent platinum(II) complexes provide an entry to new classes of 2D supramolecular nanomaterials with optoelectronic properties.

Received: October 9, 2009
Published online: November 20, 2009

Keywords: luminescence · metal–metal interactions · nanostructures · platinum · self-assembly

[1] a) A. K. Geim, K. S. Novoselov, *Nat. Mater.* **2007**, *6*, 183–191; b) C. N. R. Rao, A. K. Sood, K. S. Subrahmanyam, A. Govindaraj, *Angew. Chem.* **2009**, *121*, 7890–7916; *Angew. Chem. Int. Ed.* **2009**, *48*, 7752–7777.

[2] a) M. Van der Auweraer, F. C. De Schryver, *Nat. Mater.* **2004**, *3*, 507–508; b) S. I. Stupp, V. Le Bonheur, K. Walker, L. S. Li, K. E. Huggins, M. Keser, A. Amstutz, *Science* **1997**, *276*, 384–389; c) A. P. H. J. Schenning, E. W. Meijer, *Chem. Commun.* **2005**, 3245–3258; d) J. A. A. W. Elemans, R. van Hameren, R. J. M. Nolte, A. E. Rowan, *Adv. Mater.* **2006**, *18*, 1251–1266; e) K. Ariga, T. Nakanishi, J. P. Hill, *Curr. Opin. Colloid Interface Sci.* **2007**, *12*, 106–120.

[3] Z. Wang, Z. Li, C. J. Medforth, J. A. Shelnutt, *J. Am. Chem. Soc.* **2007**, *129*, 2440–2441.

[4] a) M. Sathish, K. Miyazawa, *J. Am. Chem. Soc.* **2007**, *129*, 13816–13817; b) T. Wakahara, M. Sathish, K. Miyazawa, C. Hu, Y. Tateyama, Y. Nemoto, T. Sasaki, O. Ito, *J. Am. Chem. Soc.* **2009**, *131*, 9940–9944.

[5] Y. Lei, Q. Liao, H. Fu, J. Yao, *J. Phys. Chem. C* **2009**, *113*, 10038–10043.

[6] R. J. Li, L. Jian, Q. Meng, J. H Gao, H. X. Li, Q. X. Tang, M. He, W. P. Hu, Y. Q. Liu, D. B. Zhu, *Adv. Mater.*, DOI: 10.1002/adma.200900934.

[7] X. J. Zhang, X. H. Zhang, B. Wang, C. Y. Zhang, J. C. Chang, C. S. Lee, S. T. Lee, *J. Phys. Chem. C* **2008**, *112*, 16264–16268.

[8] a) M. Ikeda, T. Nobori, M. Schmutz, J.-M. Lehn, *Chem. Eur. J.* **2005**, *11*, 662–668; b) R. Davis, R. Berger, R. Zentel, *Adv. Mater.* **2007**, *19*, 3878–3881; c) H. Maeda, Y. Kusunose, M. Terasaki, Y. Ito, C. Fujimoto, R. Fujii, T. Nakanishi, *Chem. Asian J.* **2007**, *2*, 350–357; d) L. Chen, J. Kim, T. Ishizuka, Y. Honsho, A. Saeki, S. Seki, H. Ihee, D. L. Jiang, *J. Am. Chem. Soc.* **2009**, *131*, 7287–7292; e) E. Lee, J.-K. Kim, M. Lee, *Angew. Chem.* **2009**, *121*, 3711–3714; *Angew. Chem. Int. Ed.* **2009**, *48*, 3657–3660.

[9] a) D. M. Roundhill, H. B. Gray, C. M. Che, *Acc. Chem. Res.* **1989**, *22*, 55–61; b) V. M. Miskowski, V. H. Houlding, *Inorg. Chem.* **1991**, *30*, 4446–4452; c) J. A. Bailey, M. G. Hill, R. E. Marsh, V. M. Miskowski, W. P. Schaefer, H. B. Gray, *Inorg. Chem.* **1995**, *34*, 4591–4599; d) C. E. Buss, C. E. Anderson, M. K. Pomije, C. M. Lutz, D. Britton, K. R. Mann, *J. Am. Chem. Soc.* **1998**, *120*, 7783–7790; e) W. R. Caseri, H. D. Chanzy, K. Feldman, M. Fontana, P. Smith, T. A. Tervoort, J. G. P. Goossens, E. W. Meijer, A. P. H. J. Schenning, I. P. Dolbnya, M. G. Debije, M. P. de Haas, J. M. Warman, A. M. van de Craats, R. H. Friend, H. Sirringhaus, N. Stutzmann, *Adv. Mater.* **2003**, *15*, 125–129; f) S. W. Lai, C. M. Che, *Top. Curr. Chem.* **2004**, *241*, 27–63.

[10] a) W. Lu, V. A. L. Roy, C. M. Che, *Chem. Commun.* **2006**, 3972–3974; b) F. Camerel, R. Ziessel, B. Donnio, C. Bourgogne, D. Guillon, M. Schmutz, C. Iacovita, J. P. Bucher, *Angew. Chem.* **2007**, *119*, 2713–2716; *Angew. Chem. Int. Ed.* **2007**, *46*, 2659–2662; c) A. Y. Y. Tam, K. M. C. Wong, G. X. Wang, V. W. W. Yam, *Chem. Commun.* **2007**, 2028–2030; d) W. Lu, S. S. Y. Chui, K. M. Ng, C. M. Che, *Angew. Chem.* **2008**, *120*, 4644–4648; *Angew. Chem. Int. Ed.* **2008**, *47*, 4568–4572; e) M. Y. Yuen, V. A. L. Roy, W. Lu, S. C. F. Kui, G. S. M. Tong, M. H. So, S. S. Y. Chui, M. Muccini, J. Q. Ning, S. J. Xu, C. M. Che, *Angew. Chem.* **2008**, *120*, 10043–10047; *Angew. Chem. Int. Ed.* **2008**, *47*, 9895–9899; f) W. Lu, K. M. Ng, C. M. Che, *Chem. Asian J.* **2009**, *4*, 830–834; g) W. Lu, Y. Chen, V. A. L. Roy, S. S. Y. Chui, C. M. Che, *Angew. Chem.* **2009**, *121*, 7757–7761; *Angew. Chem. Int. Ed.* **2009**, *48*, 7621–7625.

[11] M. Albrecht, G. van Koten, *Angew. Chem.* **2001**, *113*, 3866–3898; *Angew. Chem. Int. Ed.* **2001**, *40*, 3750–3781.

[12] For reviews on C–H$\cdots\pi$(C≡C) interactions, see: a) G. R. Desiraju, T. Steiner, *The Weak Hydrogen Bond in Structural Chemistry and Biology*, Oxford University, New York, **1999**; b) I. Alkorta, I. Rozas, J. Elguero, *Chem. Soc. Rev.* **1998**, *27*, 163–170.

[13] a) D. J. Cárdenas, A. M. Echavarren, M. C. R. de Arellano, *Organometallics* **1999**, *18*, 3337 – 3341; b) J. A. G. Williams, A. Beeby, E. S. Davies, J. A. Weinstein, C. Wilson, *Inorg. Chem.* **2003**, *42*, 8609 – 8611; c) S. J. Farley, D. L. Rochester, A. L. Thompson, J. A. K. Howard, J. A. G. Williams, *Inorg. Chem.* **2005**, *44*, 9690 – 9703.
[14] C. Baik, W.-S. Han, Y. Kang, S. O. Kang, J. Ko, *J. Organomet. Chem.* **2006**, *691*, 5900 – 5910.
[15] W. B. Connick, R. E. Marsh, W. P. Schaefer, H. B. Gray, *Inorg. Chem.* **1997**, *36*, 913 – 922.
[16] CCDC 750347, 750348, and 750349 contain the supplementary crystallographic data for this paper. These data can be obtained free of charge from The Cambridge Crystallographic Data Centre via www.ccdc.cam.ac.uk/data_request/cif.
[17] For recent examples of photoresponsive organic transistors, see: a) G. A. O'Brien, A. J. Quinn, D. A. Tanner, G. Redmond, *Adv. Mater.* **2006**, *18*, 2379 – 2383; b) H. X. Ji, J. S. Hu, L. J. Wan, *Chem. Commun.* **2008**, 2653 – 2655; c) Q. X. Tang, L. Q. Li, Y. B. Song, Y. L. Liu, H. X. Li, W. Xu, Y. Q. Liu, W. P. Hu, D. B. Zhu, *Adv. Mater.* **2007**, *19*, 2624 – 2628; d) X. F. Guo, S. X. Xiao, M. Myers, Q. Miao, M. L. Steigerwald, C. Nuckolls, *Proc. Natl. Acad. Sci. USA* **2009**, *106*, 691 – 696; e) C. Y. Zhang, X. J. Zhang, X. H. Zhang, X. M. Ou, W. F. Zhang, J. S. Jie, J. C. Chang, C. S. Lee, S. T. Lee, *Adv. Mater.* **2009**, *21*, 4172 – 4175.

